THE JOURNAL OF PHYSICAL CHEMISTRY A

pubs.acs.org/JPCA Article

2 + 2 Can Make Nearly a Thousand! Comparison of Di- and Tetra-*Meso*-Alkyl-Substituted Porphycenes

Michał Kijak, Krzysztof Nawara, Arkadiusz Listkowski, Natalia Masiera, Joanna Buczyńska, Natalia Urbańska, Grażyna Orzanowska, Marek Pietraszkiewicz, and Jacek Waluk*

Cite This: *J. Phys. Chem. A* 2020, 124, 4594–4604

Read Online

ACCESS | Metrics & More | Article Recommendations | Supporting Information

ABSTRACT: Two porphycenes, substituted at the *meso* positions with two and four methyl groups, respectively, reveal similar absorption spectra, but their photophysical properties are completely different. 9,20-dimethylporphycene emits fluorescence with about 20% quantum yield, independent of the solvent. In contrast, fluorescence of 9,10,19,20-tetramethylporphycene is extremely weak in nonviscous solvents, but it can be recovered by placing the chromophore in a rigid environment. We propose a model that explains these differences, based on calculations and structural analogies with other extremely weakly emitting derivatives, dibenzo[*cde*,*mno*]porphycenes. The efficient S_1 deactivation involves delocalization of two inner cavity protons coupled with proton translocation toward a high-energy cis tautomer. The latter process leads to distortion from planarity. The probability of deactivation increases with the strength of the intramolecular NH···N hydrogen bonds. The model also explains the observation of biexponential fluorescence decay in weakly emitting porphycenes. It can be extended to other derivatives, in particular, the asymmetrically substituted ones. We also point to the possibility of using specific porphycenes as viscosity sensors, in particular, when working in single molecule regime.

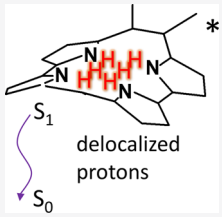

INTRODUCTION

Arguably, the majority of optical-sensing techniques are based on luminescence, fluorescence, in particular.[1,2] These techniques are widely used in various areas, ranging from biology, medicine, and pharmacology to materials and environmental sciences. Fluorescence sensors exploit the sensitivity of the emission to the environment characteristics, such as temperature, viscosity, and polarity,[3−6] or to the presence of specific analytes, for example, metal ions.[7] Obviously, a rational design of a sensor must be preceded by thorough characterization and understanding of its photophysical properties. In this work, we describe a series of compounds based on porphycene which seem to be a very good candidate for applications as viscosity sensors.

Porphycenes, structural isomers of porphyrins, have been the objects of intense investigations since the synthesis of the parent compound reported in 1986.[8] Among these studies, particularly important in terms of possible applications are those devoted to spectral and photophysical properties.[9,10] Porphycenes are very promising as sensitizers in photodynamic therapy,[11] the main, but not the only theme of numerous patents. Other areas of possible use of porphycenes based on interaction with light include photoelectrochemical devices,[12] near-IR absorbing and emitting fluorophores,[13−15] preparation of new electrochromic,[16] liquid crystalline,[17] and elastomeric[18] materials. However, comparative research on the photophysical properties of different porphycenes has been rather limited. Most of porphycenes studied until now reveal quite large fluorescence quantum yields and nanosecond decay times. A noteworthy exception is that of *meso*-tetraalkyl-substituted porphycenes, 9,10,19,20-tetramethyl-, and tetrapropyl-derivatives.[19] Room-temperature fluorescence of these molecules is extremely sensitive to solvent properties, in particular, viscosity. In low-viscosity solvents, fluorescence is extremely weak (quantum yield of 10^{-4} to 10^{-3}), whereas it dramatically increases in paraffin and even more (by about 3 orders of magnitude) for molecules embedded in polymer films. It was demonstrated that the ultrafast deactivation of the excited state is due to $S_0 \leftarrow S_1$ internal conversion, and the triplet state is not populated.[19] Moreover, specific interactions with the solvent could also be eliminated as a possible origin of this effect, because the deactivation is equally efficient in nonpolar, polar protic, and polar aprotic solvents, as long as the viscosity remains similar.

The data accumulated so far strongly suggest a link between the photophysical and tautomeric properties; the latter have been extensively investigated for porphycenes in various environments, ranging from liquid and solid condensed phases,[20−28] supersonic jets,[29−32] and helium nanodroplets,[33] to the regime of single molecules probed by fluorescence,[34−37] Raman,[38] and scanning probe microscopies.[39−45]

We have proposed the explanation of the unusual photophysical behavior of *meso*-alkylated porphycenes using a model which assumes that the species responsible for very efficient

Received: March 11, 2020
Revised: May 18, 2020
Published: May 19, 2020

Scheme 1. Tautomeric Forms of Porphycene with All Possible Transition States Linking Them Indicated[a]

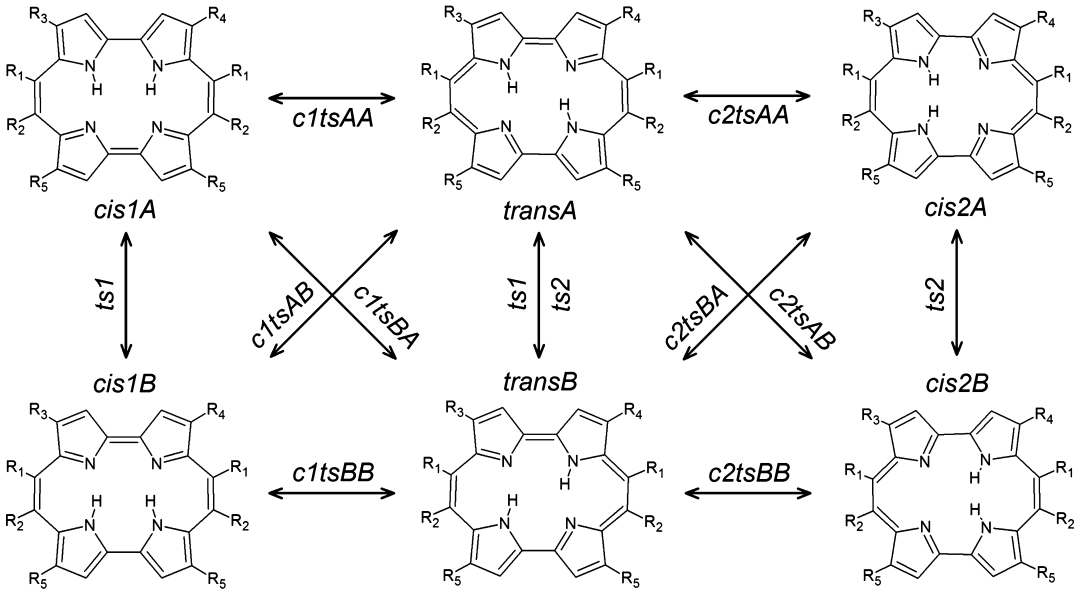

[a]For several patterns of symmetric substitution, A and B variants of some forms can be undistinguishable, and then, the A and B indices are redundant. Note that cis2 species is nonplanar.

Scheme 2. Investigated Porphycenes

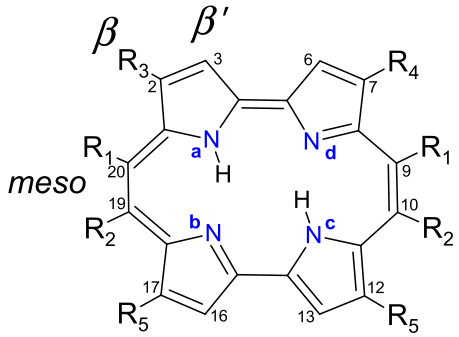

	R_1	R_2	R_3	R_4	R_5
1	H	H	H	H	H
2	Me	H	H	H	H
3	H	Me	*t*-Bu	*t*-Bu	H
4	Me	Me	H	H	H
5	Pr	Pr	H	H	H
6	H	H	*t*-Bu	H	H
7	H	H	*t*-Bu	*t*-Bu	H
8	H	H	*t*-Bu	*t*-Bu	*t*-Bu

nonradiative S_1 depopulation is a rare cis2 tautomeric form (Scheme 1).[46] In contrast to the other tautomeric species of porphycene, such a structure is nonplanar. The observed viscosity dependence can be understood by realizing that a large amplitude molecular motion resulting in distortion from planarity along the trans−cis2 tautomerization path is required to initiate rapid excited-state deactivation. Assuming that the deactivation rate is proportional to the trans(S_1)−cis2 energy difference, the calculations predicted that the efficient deactivation should increase in the order: parent porphycene, 9,20-dimethylporphycene, 2,3,6,7,12,13,16,17-octamethylporphycene, 9,10,19,20-tetramethylporphycene. This prediction was experimentally confirmed for the parent, tetra- and octa-substituted porphycenes, but the doubly substituted derivative was not known at that time. This motivated us to obtain and study 9,20-dimethylporphycene. In this work, we compare the spectral and photophysical properties of this compound (**2**) and a related, 2,7-tetra-*t*-butyl-10,19-dimethylporphycene (**3**), with the data obtained, on the one hand, for the parent porphycene (**1**), its mono- (**6**), di- (**7**), and tetra-*β*-substituted (**8**) derivatives, and, on the other hand, with the characteristics of *meso*-tetramethyl (**4**) and *meso*-tetrapropylporphycene (**5**) (Scheme 2). A spectacular finding is that removing two out of four *meso* alkyl substituents leads to a complete change in photophysics and tautomerism. In contrast to **4** and **5**, both **2** and **3** strongly fluoresce, irrespective of solvent viscosity. Moreover, only one tautomeric (trans) form is detected, in contrast to the case of *meso*-tetraalkyl-substitued porphycenes, where both trans and cis species are present. This behavior can be rationalized on the basis of calculations, which reveal very different geometry changes along the trans−cis2 pathway in **2** as compared to **4**. For the latter, a rather unusual pattern of out-of-plane bending which accompanies the trans to cis2 tautomerization is obtained. A refined model is proposed that postulates that a small distance between the H-bonded inner nitrogen atoms leads to delocalization of inner hydrogen atoms, which is responsible for efficient nonradiative S_1 depopulation. This model seems to be general, as it can also explain the biexponential fluorescence decay profiles observed in **4**, **5**, and several asymmetric porphycenes. It also accounts for the lack of fluorescence and ultrafast, temperature-independent S_1−S_0 internal conversion observed in both, planar and nonplanar dibenzo[*cde*,*mno*]porphycenes.

EXPERIMENTAL SECTION

Syntheses of **1**,[8,47] **2**−**3**,[21] **4**−**5**,[48] **6**−**7**,[49] and **8**[50] were carried out according to the procedures described in the literature.

https://dx.doi.org/10.1021/acs.jpca.0c02155
J. Phys. Chem. A 2020, 124, 4594−4604

Electronic absorption spectra were measured on Shimadzu UV 3100 and 2700 spectrophotometers. Fluorescence spectra were recorded using FS 900 CDT or FS5 spectrofluorometers (Edinburgh Instruments). The FS5 instrument was used for determination of fluorescence quantum yields of **1** in various solvents, applying a recently developed SAFE method.[51−53] The quantum yields were calculated with respect to rhodamine 6G water solution (QY = 0.92).[54,55]

The solvents used for the fluorescence measurements were of the highest available purity. Acetonitrile, *n*-hexane, dimethyl sulfoxide, methanol, ethanol, 1-butanol, toluene, liquid paraffin, and dichloromethane were acquired from Merck (Uvasol grade solvents). Dodecane, tetradecane (both with purity >99%), and methanol-d_1 (monodeuteromethanol, 99 atom % D) were purchased from Aldrich.

Fluorescence lifetimes were obtained on homebuilt setups using time-resolved single photon counting. Picoquant LDH-D-C-375 laser (379 nm, 60 ps pulse) or Fianium FemtoPower 1060 supercontinuum laser (6 ps pulses, tunable wavelength) were used as excitation sources. After passing through either (i) Digikröm CM 110 monochromator or (ii) Digikröm CM112 monochromator, the emission was detected by (i) Becker & Hickl PMC 100-4 photomultiplier and PicoQuant TimeHarp 100 PC card or (ii) Hamamatsu 3809 MCP photomultiplier or an HPM-100-40 Becker & Hickl hybrid detector and Becker & Hickl SPC-830 time-correlated single-photon-counting module. Fluorescence decays were analyzed using FAST Advanced Analysis of Fluorescence Kinetics software (Edinburgh Instruments).

Alternatively, fluorescence lifetimes were also obtained using a Becker & Hickl Simple-Tau 150 module. The emitted photons were collected by means of a multiwavelength detection system: a polychromator and a 16 channel TCSPC detector (PML-16, Becker & Hickl), which registers 16 individual fluorescence decays spanning a 200 nm spectral range (12.5 nm per channel). PicoQuant 375 nm laser diode (LDH-D-C-375) with a PDL 800-D controller was used for excitation. The impulse response function signal measured for this setup was 130 ps fwhm. The data were collected using SPCM software. The analysis of fluorescence decays was performed using SPCImage 5.0 package.

CALCULATIONS

Quantum chemical modeling of the ground and the lowest excited states was performed at the density functional theory (DFT) and time-dependent DFT (TD-DFT) levels, respectively. The hybrid B3LYP functional was used. For the excited states, we used also its long-range-corrected CAM-B3LYP version,[56] because it provides a better description of excited states with a charge-transfer character. The 6-31+G(d,p) basis set was employed.

Tautomerization reaction paths were obtained using generalized internal coordinates (GICs). The difference between distances of a moving hydrogen atom from donor and acceptor nitrogen atoms ($r_{NH}-r_{HN}$) was specified as the only one fixed and scanned coordinate. Transition states were fully optimized with TS or saddle = 2 keywords. All calculations were carried out using Gaussian 09[57] or Gaussian 16[58] suites of programs.

RESULTS AND DISCUSSION

Absorption and emission spectra of unsubstituted, parent porphycene **1**, *meso*-dimethyl derivative **2**, and *meso*-tetramethyl substituted porphycene **4** are shown in Figures 1−3. The spectra were measured in solvents of different polarity, proticity, and

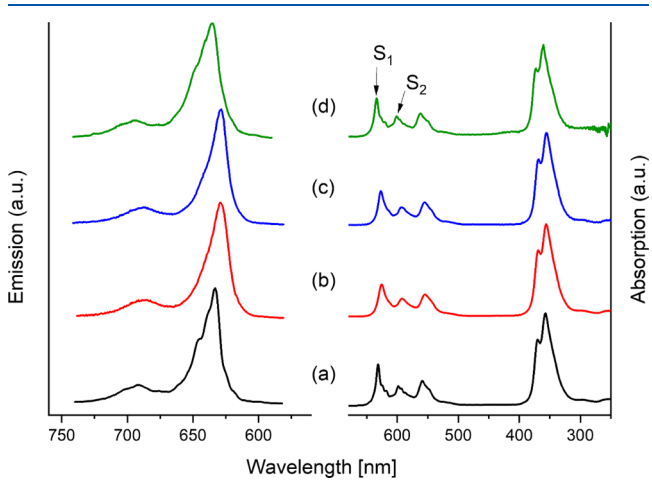

Figure 1. Room-temperature absorption and emission spectra of **1** in: (a) *n*-hexane; (b) acetonitrile; (c) methanol; (d) paraffin. The arrows mark the origins of two lowest energy electronic transitions.

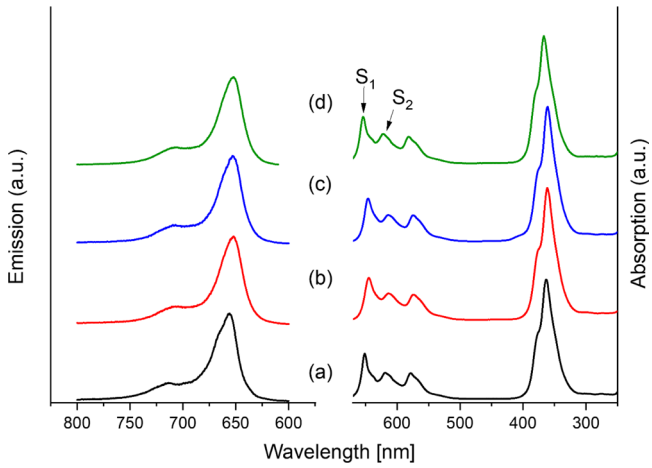

Figure 2. Room-temperature absorption and emission spectra of **2** in: (a) *n*-hexane; (b) acetonitrile; (c) methanol; (d) paraffin.

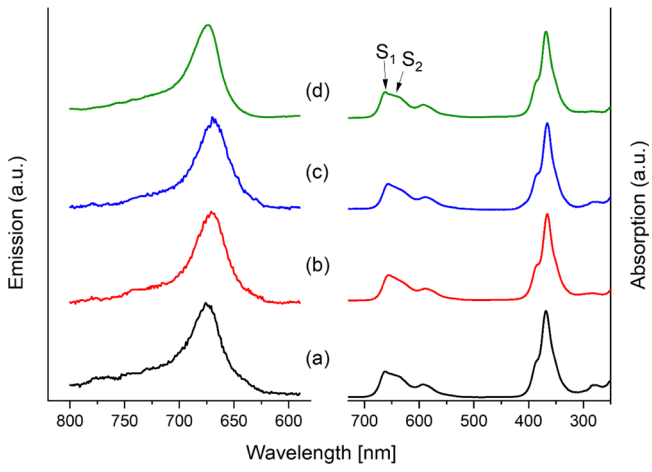

Figure 3. Room-temperature absorption and emission spectra of **4** in: (a) *n*-hexane; (b) acetonitrile; (c) methanol; (d) paraffin.

https://dx.doi.org/10.1021/acs.jpca.0c02155
J. Phys. Chem. A 2020, 124, 4594−4604

Table 1. Photophysical Parameters Obtained for Different Solvents at 293 K

	Φ_{fl}[a]	τ_{fl}[b] [ns]	k_r[c] [10^7 s^{-1}]	k_{nr}[d] [10^7 s^{-1}]	solvent
1	0.44	9.9	2.4	5.7	*n*-hexane
	0.45	10.8	2.3	5.1	acetonitrile
	0.50	9.8	2.4	5.1	DMSO
	0.41	10.4	2.3	5.7	MeOH
	0.49	11.6	2.4	4.4	MeOD
	0.43	10.3	2.3	5.5	EtOH
	0.43	10.0	2.2	5.7	BuOH
	0.49	9.6	2.3	5.3	toluene
	0.46	10.7	2.2	5.1	THF
	0.49	8.9	2.8	5.7	dichloromethane
	0.44	9.9	2.2	5.7	dodecane
	0.43	10.0	2.1	5.7	tetradecane
	0.39	10.2	1.8	6.0	paraffin
2	0.22	5.4	2.2	12.6	*n*-hexane
	0.26	6.8	2.1	10.9	acetonitrile
	0.25	5.8	2.5	12.9	methanol
	0.18	5.5	1.8	14.9	paraffin
3	0.19	4.5	2.3	18.0	*n*-hexane
	0.21	5.0	2.3	15.8	acetonitrile
	0.18	3.8	2.7	21.6	methanol
	0.19	4.9	1.8	16.5	paraffin
4	2.9×10^{-4}	0.003/0.017[e]	1.4	9997	cyclohexane
	3.4×10^{-4}				acetonitrile
	6.0×10^{-4}				butanol
	1.5×10^{-3}				DMSO
	4.2×10^{-3}	0.20/0.40[f]	0.9	331	paraffin
5	5.4×10^{-4}	0.008/0.036[f]	1.2	4543	cyclohexane
	8.1×10^{-4}	0.006/0.030[f]			acetonitrile
	5.3×10^{-4}				methanol
	3.5×10^{-3}				DMSO
		0.5/1.1[f]			paraffin
6	0.37	10.7	1.9	5.9	*n*-hexane
	0.43	10.2	2.4	5.6	acetonitrile
7	0.43	10.3	2.3	5.5	*n*-hexane
	0.39	10.5	2.1	5.8	acetonitrile
8	0.38	8.4	2.5	7.4	*n*-hexane
	0.44	9.3	2.6	6.0	acetonitrile

[a]Fluorescence quantum yields at room temperature. [b]Fluorescence decay times at room temperature, estimated accuracy ±0.2 ns. [c]Radiative constants of S_1 depopulation, including n^2 correction. [d]Sum of nonradiative depopulation constants. [e]Reference 66. [f]Reference 19.

viscosity. For each compound, solvent dependence of the band shape and position is very weak, both in absorption and fluorescence. As could have been expected, the spectra are somewhat better structured in nonpolar solvents.

Alkyl substitution at the *meso* position results in a moderate red shift that scales in the approximately linear fashion with the number of substituents. Thus, the S_0-S_1 transition energy in **2** lies about 400 cm^{-1} lower than in **1**, whereas the difference between **4** and **1** amounts to ca. 800 cm^{-1}. These trends are correctly predicted by TD-DFT calculations.

The additivity breaks down completely with respect to the photophysical parameters (Table 1). Double *meso* substitution leads to approximately 50% reduction in fluorescence quantum yield and lifetime. In contrast, upon adding two more methyl groups fluorescence intensity decreases dramatically. For instance, the quantum yields of **1** and **4** in *n*-hexane or acetonitrile differ by 3 orders of magnitude. We have previously reported very low fluorescence quantum yield of **4** and **5** and detected that the emission of *meso*-tetraalkyl-substituted porphycenes is crucially dependent on solvent viscosity.[19] In a rigid environment, obtained by freezing the solution or, alternatively, by embedding the chromophore in a polymer matrix at room temperature, fluorescence intensity and lifetime largely increase, reaching the values comparable with those obtained for **2**. On the other hand, Table 1 shows that the emission of the doubly substituted porphycene **2** does not exhibit any viscosity dependence, revealing the same quantum yield in nonviscous *n*-hexane and in viscous paraffin.

We have also synthesized another derivative, 2,7-tetra-*t*-butyl-10,19-dimethylporphycene (**3**), bearing four alkyl substituents in a different arrangement than in **4** and **5**: two at the *meso* and two at the β positions. The photophysical properties of **2** and **3** are practically the same (Table 1): both molecules show quite strong fluorescence, not sensitive to solvent viscosity, polarity, and proticity.

Similar photophysical behavior has been observed for porphycenes substituted with one, two, and four *tert*-butyl groups at the β positions (molecules **6**, **7**, and **8**, respectively). All these porphycenes fluoresce nearly as efficiently as

https://dx.doi.org/10.1021/acs.jpca.0c02155
J. Phys. Chem. A 2020, 124, 4594−4604

Table 2. (TD-) (CAM-)B3LYP/6-31+G(d,p) Calculated Energies (E), Dipole Moments (μ), Inner Cavity Sizes (N_x−N_y), and NH Stretching Frequencies (ν_{NH}) of Different Tautomeric Forms and Transition States of 1−8 in the Ground and Lowest Excited Electronic States (nπ* and $\pi\pi$* for the cis2 Form if Possible)

	Form[a]		E [kcal/mol]								Nx-Ny[e] (x-y) distance [pm]												μ [D]			ν_{NH}[f] [cm^{-1}]	
			S_0 B3LYP		S_1 B3LYP			S_1 CAM-B3LYP			S_0 B3LYP				S_1 B3LYP				S_1 CAM-B3LYP				S_0	S_1	S_1[C]	S_0	
			S_0[b]		S_1	S_1[b,c]	S_0[d]	S_1	S_1[b,c]	S_0[d]	a-b	c-d	a-d	b-c	a-b	c-d	a-d	b-c	a-b	c-d	a-d	b-c				sym	asym
1	*ts1*	D_{2h}	6.48 (1.10)		57.5	7.33 (2.22)	8.1	55.5	6.95 (1.83)	8.1	250	250	291	291	250	250	293	293	250	250	291	291	0.00	0.00	0.00	-1221	-1084
	trans	C_{2h}	0.00 (0.00)		50.1	0.00 (0.00)	1.3	48.5	0.00 (0.00)	0.9	266	266	284	284	269	269	285	285	267	267	284	284	0.00	0.00	0.00	2916	2916
	c1ts	C_s	4.28 (1.30)		54.8	4.69 (1.98)	5.8	53.0	4.49 (1.70)	5.5	259	252	290	287	260	252	292	289	259	252	291	287	0.69	0.59	0.72	-1212	2617
	cis1	C_{2v}	2.30 (1.74)		52.1	1.99 (1.67)	3.9	50.7	2.13 (1.55)	3.1	262	262	289	284	264	264	291	285	262	262	290	284	1.31	1.20	1.54	2677	2640
	c2ts	C_s	43.4 (40.7)		92.3	42.1 (39.3)	49.8	91.9	43.4 (40.8)	44.7	303	309	240	269	308	312	241	271	304	308	240	268	1.08	1.81	1.51	3661	-1605
	cis2	C_2	29.5 (29.4)	nπ*	72.3	22.2 (23.5)	49.7	nπ*	78.3	29.8 (30.9)	54.1	291	303	270	270	250	275	296	296	242	272	299	299	1.92	1.67	0.72	3627	3622
		C_2						ππ*	77.2	28.7 (28.6)	31.1									292	299	272	272			2.87		
2	*ts1*	C_{2v}	5.60 (0.52)		54.1	6.22 (1.29)	7.3	52.1	5.98 (0.93)	7.4	249	249	295	289	250	250	296	291	249	249	295	289	0.13	0.36	0.44	-1188	-1052
	trans	C_s	0.00 (0.00)		47.9	0.00 (0.00)	1.6	46.2	0.00 (0.00)	1.4	264	264	289	282	265	266	290	283	264	264	289	282	0.18	0.40	0.39	2837a	2880c
	c1tsA	C_s	3.45 (0.66)		52.1	4.22 (1.48)	5.1	50.2	4.06 (1.16)	4.8	257	251	295	285	258	251	296	287	257	251	295	286	0.76	0.90	1.06	-1184	2556
	cis1A	C_{2v}	1.44 (1.16)		50.0	2.07 (1.79)	3.0	48.4	2.21 (1.50)	2.2	260	260	294	282	261	261	295	283	260	260	294	282	1.32	1.47	1.81	2603	2566
	c1tsB	C_s	3.95 (1.08)		51.7	3.78 (1.13)	5.7	49.8	3.63 (0.89)	5.6	251	257	292	288	252	259	293	290	251	258	292	288	0.43	0.21	0.22	-1153	2581
	cis1B	C_{2v}	2.37 (1.95)		49.1	1.24 (1.13)	4.2	47.5	1.31 (0.94)	3.6	260	260	289	288	262	262	290	289	261	261	289	287	0.91	0.78	0.95	2614	2577
	c2tsAA	C_s	43.7 (41.3)		90.4	42.5 (39.7)	49.4	90.6	44.5 (41.3)	45.1	297	303	277	240	301	306	278	240	298	302	276	239	1.10	1.72	1.57	3668	-1569
	c2tsAB	C_s	49.9 (47.7)		C_1 97.4	49.5 (46.8)	52.4	96.7	50.5 (48.1)	50.9	305	299	245	266	304	299	243	266	304	301	244	265	0.99	1.57	1.42	3663	-1689
	cis2	C_1	30.7 (30.7)	nπ*	70.0	22.2 (23.8)	52.1	nπ*	75.4	29.2 (30.6)	56.7	286	297	279	269	245	271	304	295	237	269	308	298	1.83	1.68	0.66	3632d	3617c
		C_1						ππ*	76.5	30.3 (30.1)	32.4									285	291	282	273			2.84		
3	*trans*	C_s	0.00 (0.00)		47.4	0.00 (0.00)	1.7	45.7	0.00 (0.00)	1.4	264	264	287	289	266	265	288	290	264	264	287	289	0.94	0.75	0.55	2838c	2811a
	cis1B	C_{2v}	1.46 (1.02)		49.2	1.79 (1.30)	3.1	47.9	2.21 (1.29)	2.0	261	261	287	293	262	262	288	295	260	260	287	294	0.27	0.40	0.99	2624	2589
	cis1A	C_{2v}	2.32 (1.69)		48.7	1.29 (0.97)	4.1	46.9	1.17 (0.75)	3.6	260	260	292	289	262	262	293	289	261	261	292	288	2.10	1.87	1.88	2565	2530
	cis2	C_1	31.9 (32.1)		71.0	23.6 (25.1)	53.3	nπ*	76.1	30.4 (31.8)	58.2	285	296	275	278	244	271	302	303	236	269	305	306	2.18	1.84	0.99	3629c	3625d
		C_1						ππ*	77.2	31.5 (31.3)	33.3									285	291	279	281			3.25		
4	*ts1*	D_2	3.88 (-1.20)		52.2	4.57 (-0.52)	6.4	50.1	4.42 (-0.65)	6.5	248	248	296	296	248	248	296	296	247	247	295	295	0.00	0.00	0.00	-1098	-957
	trans	C_2	0.00 (0.00)		47.6	0.00 (0.00)	2.1	45.7	0.00 (0.00)	2.0	258	258	291	291	260	260	291	291	259	259	290	290	0.07	0.07	0.08	2669	2678
	ts1	C_{2h}	3.90 (-1.14)								248	248	296	296									0.00			-1099	-958
	trans	C_i	0.03 (0.02)		47.7	0.13 (-0.03)	2.3	45.8	0.11 (0.10)	2.1	258	258	292	292	260	260	291	291	259	259	290	290	0.00	0.00	0.00	2670	2679
	c1ts	C_1	2.55 (-0.30)		50.5	2.89 (0.13)	5.0	48.4	2.80 (-0.02)	4.9	254	249	296	293	255	249	296	293	254	249	294	292	0.59			-1074	2436
	cis1	C_2	1.45 (0.79)		48.8	1.25 (0.80)	3.8	47.0	1.30 (0.60)	3.3	255	255	295	291	258	258	296	290	256	256	294	289	1.07	0.97	1.14	2446	2408
	c1ts	C_1	2.58 (-0.26)								254	249	296	293									0.59	0.48	0.54	-1073	2434
	cis1	C_s	1.48 (0.80)		48.9	1.28 (0.90)	3.8	47.0	1.34 (0.67)	3.3	255	255	296	291	258	258	296	290	256	256	295	289	1.07	0.97	1.15	2444	2406
	c2ts	C_1	50.7 (47.9)								284	289	241	273									1.08			3685	-1605
	cis2	C_2	32.5 (32.8)	nπ*	67.4	19.8 (22.4)	58.4	nπ*	70.9	25.2 (28.0)	63.7	279	287	286	286	233	267	309	309	226	266	312	312	1.27	1.60	0.14	3633	3636
5	*trans*	C_2	0.00 (0.00)		46.9	0.00 (0.00)	1.6	44.7	0.00 (0.00)	1.3	257	257	291	291	259	259	292	292	258	258	291	291	0.01	0.06	0.04	2654	2663
	cis	C_2	1.33 (0.79)		48.0	1.07 (0.77)	3.0	45.9	1.20 (0.55)	2.3	255	255	295	291	257	257	296	292	256	256	290	295	0.98	0.92	1.10	2443	2405
	cis2	C_2	33.1 (34.0)	nπ*	66.9	20.0 (23.1)	58.7	nπ*	71.0	26.4 (29.2)	63.7	277	284	288	288	233	265	308	308	226	264	312	312	1.80	1.74	0.42	3633	3636
6	*transA*	C_s	0.00 (0.00)								266	267	286	283									0.96			2898a	2909c
	transB	C_s	0.46 (0.52)								265	267	287	284									0.80			2937b	2887d
	cis1A	C_s	2.50 (1.88)								261	263	292	284									2.05			2638a	2601d
	cis1B	C_s	2.49 (2.03)								261	263	286	289									0.93			2685b	2622c
	cis2B	C_1	29.9 (29.8)								292	302	273	269									1.49			3630c	3618d
	cis2A	C_1	30.3 (30.1)								304	290	273	269									2.69			3636a	3608b
7	*trans*	C_s	0.0 (0.0)								267	267	289	283									1.15			2876a	2933c
	cis1A	C_{2v}	2.21 (1.64)								262	262	294	283									2.50			2619	2584
	cis1B	C_{2v}	2.33 (1.79)								262	262	289	289									0.23			2688	2653
	cis2	C_1	30.3 (30.4)								291	302	276	268									2.39			3632d	3617c
8	*trans*	C_{2h}	0.0 (0.0)		48.8	0.00 (0.00)	1.6	47.1	0.00 (0.00)	0.9	267	267	288	288	269	269	289	289	267	267	288	288	0.00	0.00	0.00	2885	2888
	cis1	C_{2v}	2.07 (1.53)		50.5	1.68 (1.28)	3.8	49.0	1.90 (1.28)	2.7	263	263	293	288	269	269	289	289	263	263	288	293	1.44	1.19	1.63	2646	2613
	cis2	C_2	31.1 (31.4)	nπ*	73.6	24.8 (26.3)	51.2	nπ*	79.2	32.1 (33.5)	56.1	291	302	275	275	250	274	301	301	241	271	305	305	2.25	1.75	0.55	3628	3626
		C_2						ππ*	77.7	30.6 (30.7)	32.1									291	298	276	276			3.40		

[a]Tautomeric form, see Scheme 1, and its symmetry. [b]Zero-point vibrational energy corrected values in brackets (scaling factors 0.964 and 0.952 for B3LYP and CAM-B3LYP, respectively). [c]Relative energies. [d]Vertical energies. [e]See Scheme 2 for nitrogen atoms lettering. [f]Symmetric and asymmetric stretching modes for symmetrical systems; for asymmetrical ones, the letters indicate NH nitrogen atoms. Negative values correspond to imaginary frequencies characterizing transition states.

porphycene **1** (Table 1). As in the cases of **2** and **3**, no significant solvent dependence could be detected.

These results imply that the huge decrease of fluorescence intensity observed for **4** and **5** is an effect specific for *meso* substitution. What needs to be explained, however, is the complete lack of additivity: the drastic reduction of fluorescence intensity is only observed for porphycenes with four alkyl groups, but not when two such substituents are present at the *meso* positions.

As mentioned in the Introduction section, calculations based on the model of deactivation involving the role of the nonplanar cis2 tautomer predicted that the fluorescence should decrease in the order **1** > **2** > **4**.[46] However, because only the stationary structures were considered, the reaction path leading from the initially excited form to the species that is rapidly deactivated remained unknown. We have, therefore, attempted to carry out calculations aiming to elucidate the mechanism of photo-induced tautomerization, in order to understand the completely different photophysics of doubly and quadruply *meso*-substituted porphycenes. The goal was to compare trans−cis1 and trans−cis2 paths in dimethyl-substituted porphycene **2** and tetramethyl derivative **4**. The results of calculations are presented in Table 2 and Figure 4.

The obtained trans−cis1 tautomerization profiles are similar in the two molecules, both in S_0 and S_1. In contrast, a dramatic difference was revealed for the trans−cis2 conversion. Figure 5 compares geometry changes calculated for the ground state of **2** and **4** along the trans−cis2 tautomerization path. A completely different picture is obtained for the two molecules. The dimethyl derivative **2** remains planar until the moving hydrogen is

https://dx.doi.org/10.1021/acs.jpca.0c02155
J. Phys. Chem. A 2020, 124, 4594−4604

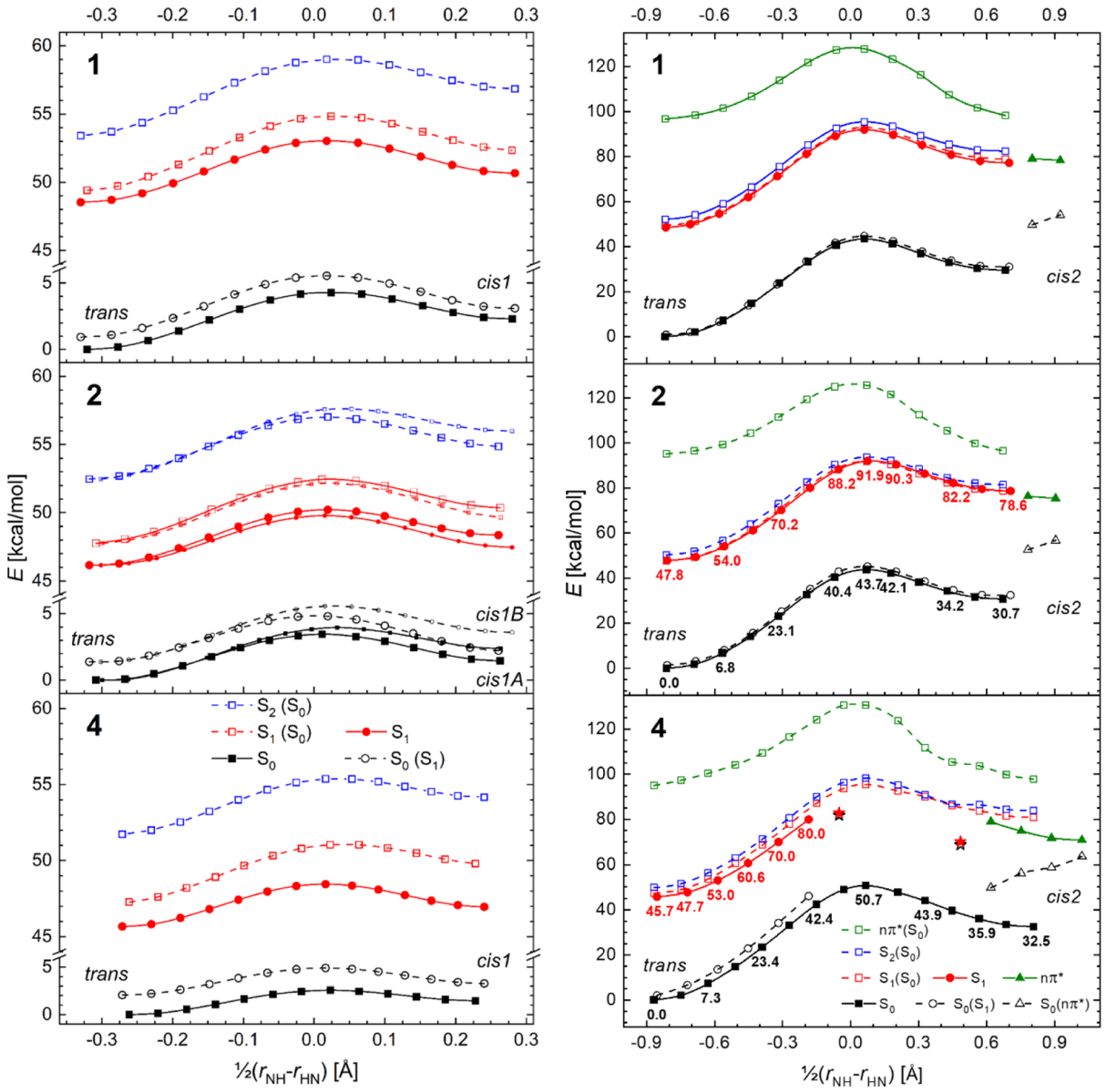

Figure 4. Potential energy profiles calculated for trans−cis1 and trans−cis2 tautomerization reactions of **1**, **2**, and **4** in S_0 (B3LYP), S_1, and nπ* (CAM-B3LYP) states. Solid lines/full symbols correspond to energies of the optimized state, while dashed lines/open symbols are vertical excitation energies. Stars mark first points on trans and cis2 sides of the trans−cis2 S_1 optimized curve for **4** for which the TD-DFT approach breaks down because of near degeneracy of S_0 and S_1 states. See also Figure 5 for the geometries along the trans−cis2 path.

transferred to the other nitrogen atom. Then, as expected, two pyrrole rings assume an out-of-plane conformation, with the two NH bonds pointing upward and downward, respectively (cf. also Scheme 1).

In contrast, while the optimized cis2 form of tetramethylporphycene **4** has essentially the same structure as in **2**, the path leading to it from the trans species is completely different. Already at the initial stage of hydrogen transfer, the molecule becomes strongly nonplanar, assuming a saddle-like shape (Figure 5).

The trans−cis2 energy profile calculated for **2** in S_1 is similar to that obtained for S_0 (Figure 4). On the other hand, the full S_1 tautomerization profile could not be obtained for **4** because the energy was not converging, even before reaching the maximum along the reaction path. The molecule was becoming strongly bent, and its ground-state energy was going strongly upward, leading to a very small S_0−S_1 energy gap. This behavior, suggesting the presence of S_1−S_0 conical intersection, which TD-DFT calculations are not able to handle properly, could have been expected. It should also be noted that the S_1−S_2 energy gap in *meso*-tetraalkylporphycenes is very small (<700 cm^{-1} compared to ca. 1000 cm^{-1} in parent porphycene[59]). The situation can be even more complicated: the orbital nature of the optimized form of cis2 in the lowest excited state of **4** was found to correspond to an nπ* transition, of which the energy significantly decreases as the hydrogen atom migrates from the trans to the cis2 tautomer. This close proximity of several electronic transitions, combined with the size of the molecule, makes the computational task of finding the structure responsible for efficient S_1−S_0 deactivation extremely challenging, if not impossible. Our future plans include search for conical intersections using such methods as, for example, computationally relatively inexpensive spin-flip TD-DFT.

https://dx.doi.org/10.1021/acs.jpca.0c02155
J. Phys. Chem. A 2020, 124, 4594−4604

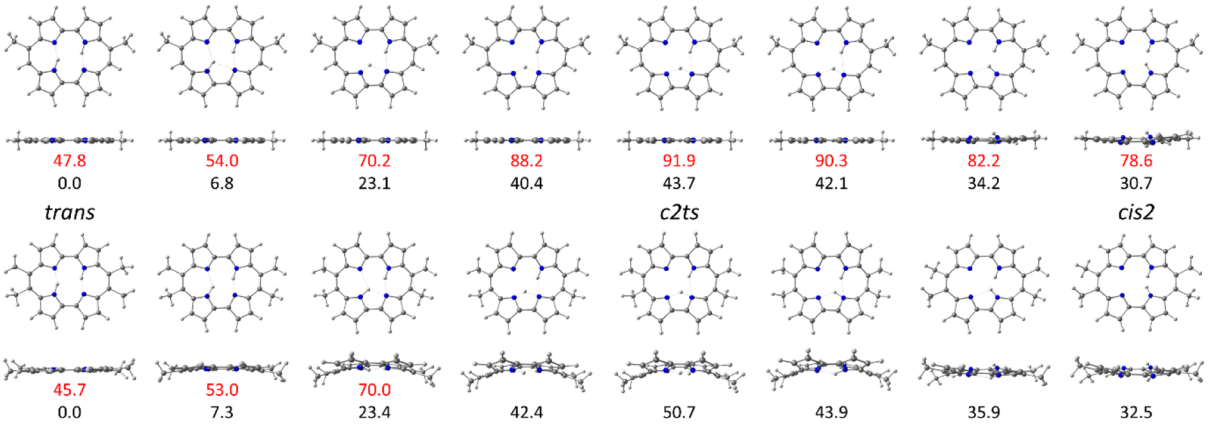

Figure 5. Calculated geometry changes that accompany trans−cis2 tautomerization in the ground electronic state of **2** (top) and **4** (bottom). The numbers below each structure indicate relative energies with respect to the ground state of the trans form. The top row (in red) corresponds to the S_1 state. See Figure 4 for energy profiles.

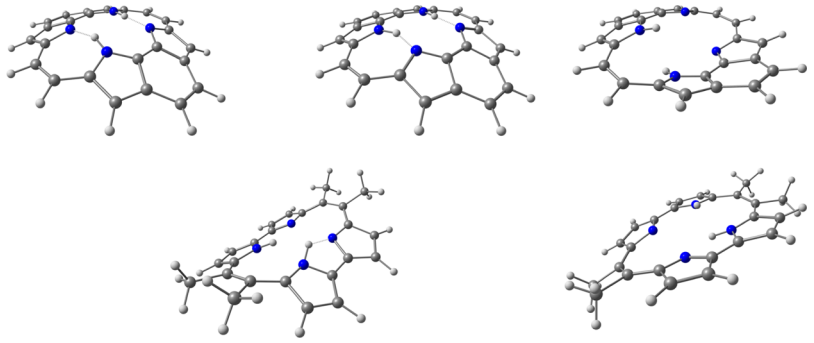

Figure 6. Top, optimized structures of trans, cis1, and cis2 forms of dibenzo[*cde*,*mno*]por-phycene. Bottom, nonplanar geometry of **4** calculated along the path of trans−cis2 conversion in S_0 (left, see also Figure 4) and the optimized cis2 form.

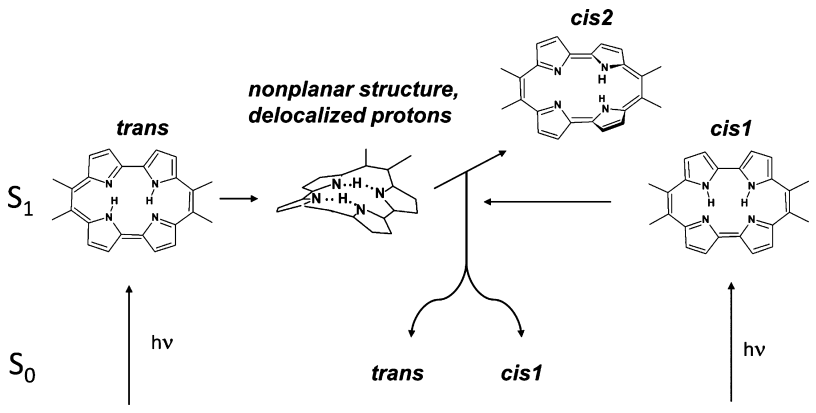

Figure 7. Tautomerization processes in S_1, leading to efficient excited-state depopulation.

In terms of explaining the nature of the ultrafast depopulation of excited *meso*-tetraalkylporphycenes, the most significant result is the nonplanar structure of **4** along the trans−cis2 tautomerization path. Close inspection of the nonplanar geometry reveals structural similarity to 3,6-13,16-dibenzo-[*cde*,*mno*]porphycene (Figure 6), of which two derivatives, 2,7,12,17-tetramethyl- and 2,7,12,17-tetra-*tert*-butyl-, have been experimentally investigated in our laboratory.[60,61] Both were found to be nonemissive, not only at room, but also at cryogenic temperatures. Picosecond transient absorption studies revealed that the recovery of the ground-state population via S_1−S_0 internal conversion occurs in 10−20 ps in a rigid argon matrix at 27 K. Interestingly, dibenzoporphycene substituted with four methyl groups is not planar, but the tetra-*tert*-butyl analogue is. This indicates that the nonplanarity is not a necessary requirement for efficient excited-state deactivation. What matters is the very small distance between the nitrogen atoms, which results in a very strong hydrogen bond and, finally, proton delocalization. Indeed, while the calculations performed for dibenzoporphycenes predict a double minimum potential with extremely small barriers for trans−trans, cis1−cis1, and cis1−trans conversions (Table S1), inclusion of zero-point energies results in delocalization of both inner hydrogen atoms.

Based on the above experimental and theoretical findings, we propose that delocalization of inner hydrogens is responsible for the efficient S_1 deactivation in porphycenes. Once the structure

https://dx.doi.org/10.1021/acs.jpca.0c02155
J. Phys. Chem. A 2020, 124, 4594−4604

with delocalized inner hydrogens has been achieved, the molecule undergoes fast $S_0 \leftarrow S_1$ radiationless transition (Figure 7). The probability of obtaining the appropriate geometry is a strong function of the NH···N distance and is the largest in dibenzoporphycenes, for which this distance is the shortest (2.51 Å). In this case, the ground-state geometry, planar or not, ensures rapid S_1 depopulation. Therefore, lowering of temperature and/or placing the molecule in a rigid environment has no effect on the emission, which is weak under any conditions. In contrast, in *meso*-tetraalkylporphycenes, NH···N separation is slightly larger (2.53 Å) and, in order to reach the "delocalized" geometry, distortion from planarity is required (cf. Figure 5). Because this distortion represents a large amplitude motion, one can expect viscosity dependence, exactly as observed experimentally.

Our model can explain another, rather intriguing finding: observation of biexponential emission decay in **4**, with the lifetimes increasing from picoseconds to nanoseconds upon passing from solutions to a rigid environment. We can now propose that these lifetimes reflect the times required to reach the point of efficient S_1 depopulation from the initially excited trans and cis1 species. Naturally, as the solvent is getting more viscous, the probability of reaching the nonplanar configuration decreases.

The proposed scheme of S_1 deactivation is similar to the model put forward by Nonell and co-workers in order to explain the photophysics of asymmetric porphycenes.[24,62] Analyzing the properties of 9-substituted *n*-propyl and methoxyethylporphycenes, they came to the conclusion that "tautomerization is coupled with an efficient deactivation pathway".[24] The cis2 tautomer was postulated as the species responsible for efficient S_1 deactivation.[62] Our present results indicate that deactivation may occur along the trans−cis2 tautomerization coordinate before reaching the relaxed cis2 structure. Such a process is resemblant of fluorescence quenching by "unsuccessful" or "aborted" chemical reaction, a theoretical model proposed by Olivucci and co-workers.[63]

One should note that hydrogen delocalization, which we postulate to be crucial for S_1 deactivation, occurs between trans and cis1 forms, which can be illustrated by the vertical movement of one of the protons in Scheme 1, but the efficient radiationless transition is triggered by the proton movement toward cis2, that is, in the horizontal directions. Such situation is not unusual. It has been demonstrated by calculations that the proton density in hydrogen bonds may have a disc-like shape, with the plane of the disc perpendicular to the H-bond axis.[64]

SUMMARY AND CONCLUSIONS

Experimental and theoretical results clearly indicate the link between the unusual photophysical behavior and tautomeric properties of porphycenes, as illustrated by the scheme of excited scheme tautomerism in *meso*-tetraalkylated porphycenes, as shown in Figure 7. We demonstrated earlier that in the electronic ground state of **4** and **5**, trans and cis1 tautomers coexist in about 4:1 ratio.[19] In the same work, it was found that (i) the excited state decay is slower than trans−trans conversion (picoseconds vs 100 fs or less, respectively) and that (ii) no equilibrium between trans and cis1 is established in S_1, as demonstrated by bi-exponential fluorescence decay. These observations were explained by the multidimensional character of the tautomerization coordinate, involving the rotation of the alkyl moiety. We now refine this model, postulating that the probability of rapid S_1 depopulation should, in general, increase with the strength of intramolecular H-bonds and therefore need not be substituent-specific. In fact, efficient deactivation can be expected for any substituent that modifies the inner cavity dimensions in a way that leads to a stronger H-bond. This hypothesis is experimentally confirmed by our ongoing research on mixed *meso* aryl/alkyl as well as halogenated porphycenes.

In the present model, the distance between the H-bonded N atoms seems to be a crucial parameter that determines the probability of fast excited state deactivation. We note, however, that low fluorescence quantum yields (albeit about an order of magnitude higher than in **4** and **5**) have been found also for porphycenes substituted with eight alkyl groups on the pyrrole rings. In these molecules, the NH···N distances are significantly larger than those in "normally" emitting porphycenes, 2.80 versus ca. 2.60 Å[10] (see also Table S1). However, the octaalkyl derivatives were found to be nonplanar in S_0. Moreover, the "horizontal" N···N distance is now smaller than that in other porphycenes. These factors can partially compensate the effect of weak H-bonds.

The two fluorescence decay times observed in **4** and **5**, assigned to the decay of trans and cis1 forms, indicate that these tautomeric forms are not in equilibrium. This strongly suggests that the excited-state trans−cis1 tautomerization path cannot bypass the molecular geometry responsible for the efficient internal conversion to S_0. If this were to be the case, the trans−cis1 equilibrium would be established for the overwhelming majority of excited molecules in the time much shorter than the experimentally measured fluorescence decays, in particular, those obtained for viscous solvents.

Unfortunately, it was not possible to safely assign each of the decay components in **4** and **5** to a specific form by selectively exciting and probing at specific wavelengths because both absorption and emission of trans and cis1 lie at practically the same energies (calculations predict a difference of only 100 cm^{-1} for S_0-S_1 transitions in the two tautomers).

The scheme presented in Figure 7 is quite general. We believe that it can be applied for both symmetrically and asymmetrically substituted porphycenes. For the latter, it is natural to assume that the trans−trans tautomerization occurs in a stepwise fashion with the cis1 intermediate, because the two intramolecular NH···N bonds have different strengths. Also, in symmetric derivatives, the stepwise mechanism should be favored at high temperatures, as demonstrated recently by nuclear quantum dynamics calculations.[65]

In order to further test the present model, it would be instructive to find other arguments for proton delocalization. As of now, we note a significant difference in the absorption spectra of **4** recorded in the Q region for two isotopomers: the nondeuterated molecule and the species with two inner protons replaced by deuterons.[19] The spectra are much broader and less-structured in the former. For parent porphycene, such an effect is not observed. Another relevant feature is the activation energy of the process responsible for temperature dependence of fluorescence determined for **4** and **5** in the MeOH/EtOH and MeOD/EtOD mixtures. For both molecules, a larger value was obtained for deuterated solvents.[19]

Finally, we consider a possibility of using custom-designed porphycenes as viscosity sensors. It may at first appear unrealistic because the fluorescence quantum yields of viscosity-sensitive porphycenes are quite low. However, when single molecule fluorescence sensors are considered, the crucial factor is not the emission quantum yield, but the yield of triplet formation and the triplet lifetime. A molecule trapped in the dark

https://dx.doi.org/10.1021/acs.jpca.0c02155
J. Phys. Chem. A 2020, 124, 4594−4604

"OFF" state does not emit fluorescence. Because the triplet lifetimes are of the order of several hundred microseconds under typical conditions of single molecule experiments (thin polymer film at room temperature), the number of photons emitted per time unit is drastically reduced for chromophores with considerable yields of triplet formation. It is instructive, in this context, to compare strongly emitting **1** with weakly emitting **4** and **5**. Parent porphycene **1** has the fluorescence quantum yield of ca. 50% and a similar yield of triplet formation, whereas **4** or **5** emit fluorescence with quantum yields of ca. 10^{-3}, but they exhibit negligible triplet formation yields. It can be readily simulated (assuming the triplet lifetime of 200 μs, a value we know from the experiment) that the number of photons emitted per time unit in the single molecule regime will be orders of magnitude larger for seemingly "weaker" luminophores. An additional advantage of these molecules may be higher photostability, because photodecomposition usually involves the triplet state.

Other obvious advantages of porphycenes are: (i) large scale of fluorescence intensity changes with solvent viscosity; (ii) insensitivity to temperature (similar intensities and lifetimes for low temperature glasses and room temperature polymer matrices); (iii) insensitivity to solvent polarity (although this may not be true for certain porphycenes); (iv) strong absorption in the convenient spectral region; (v) emission located in the red part of the visible range. Initial studies indicate that porphycene **4** fulfills all the above criteria. A particularly attractive variant may involve combining two porphycenes, such as, for example, **2** and **4**, that differ dramatically in the dependence of fluorescence quantum yield on viscosity, otherwise being very similar. Such a sensor could work in the ratiometric mode, enhancing sensitivity and accuracy.

■ ASSOCIATED CONTENT

Supporting Information

The Supporting Information is available free of charge at https://pubs.acs.org/doi/10.1021/acs.jpca.0c02155.

Calculated structural and spectral parameters for several porphycenes (PDF)

■ AUTHOR INFORMATION

Corresponding Author

Jacek Waluk − *Institute of Physical Chemistry, Polish Academy of Sciences, 01-224 Warsaw, Poland; Faculty of Mathematics and Science, Cardinal Stefan Wyszyński University, 01-815 Warsaw, Poland;* orcid.org/0000-0001-5745-583X; Email: jwaluk@ichf.edu.pl

Authors

Michał Kijak − *Institute of Physical Chemistry, Polish Academy of Sciences, 01-224 Warsaw, Poland*

Krzysztof Nawara − *Institute of Physical Chemistry, Polish Academy of Sciences, 01-224 Warsaw, Poland; Faculty of Mathematics and Science, Cardinal Stefan Wyszyński University, 01-815 Warsaw, Poland;* orcid.org/0000-0002-3847-4856

Arkadiusz Listkowski − *Institute of Physical Chemistry, Polish Academy of Sciences, 01-224 Warsaw, Poland; Faculty of Mathematics and Science, Cardinal Stefan Wyszyński University, 01-815 Warsaw, Poland*

Natalia Masiera − *Institute of Physical Chemistry, Polish Academy of Sciences, 01-224 Warsaw, Poland*

Joanna Buczyńska − *Institute of Physical Chemistry, Polish Academy of Sciences, 01-224 Warsaw, Poland*

Natalia Urbańska − *Institute of Physical Chemistry, Polish Academy of Sciences, 01-224 Warsaw, Poland*

Grażyna Orzanowska − *Institute of Physical Chemistry, Polish Academy of Sciences, 01-224 Warsaw, Poland*

Marek Pietraszkiewicz − *Institute of Physical Chemistry, Polish Academy of Sciences, 01-224 Warsaw, Poland*

Complete contact information is available at: https://pubs.acs.org/10.1021/acs.jpca.0c02155

Notes

The authors declare no competing financial interest.

■ ACKNOWLEDGMENTS

This work was supported by the Polish National Science Centre (NCN) grant 2016/22/A/ST4/00029, the PL-Grid Infrastructure grant, and the computing grant from the Interdisciplinary Centre for Mathematical and Computational Modeling.

■ REFERENCES

(1) Demchenko, A. P. *Introduction to Fluorescence Sensing*; Springer International Publishing Switzerland, 2015.

(2) Demchenko, A. P. Nanoparticles and nanocomposites for fluorescence sensing and imaging. *Methods Appl. Fluoresc.* **2013**, *1*, 022001.

(3) Vyšniauskas, A.; Kuimova, M. K. A twisted tale: measuring viscosity and temperature of microenvironments using molecular rotors. *Int. Rev. Phys. Chem.* **2018**, *37*, 259−285.

(4) Vyšniauskas, A.; Lopez-Duarte, I.; Thompson, A. J.; Bull, J. A.; Kuimova, M. K. Surface functionalisation with viscosity-sensitive BODIPY molecular rotor. *Methods Appl. Fluoresc.* **2018**, *6*, 034001.

(5) Lee, S.-C.; Heo, J.; Woo, H. C.; Lee, J.-A.; Seo, Y. H.; Lee, C.-L.; Kim, S.; Kwon, O.-P.; Kim, S.; Kim, S. Fluorescent molecular rotors for viscosity sensors. *Chem.—Eur. J.* **2018**, *24*, 13706−13718.

(6) Sedgwick, A. C.; Wu, L.; Han, H.-H.; Bull, S. D.; He, X.-P.; James, T. D.; Sessler, J. L.; Tang, B. Z.; Tian, H.; Yoon, J. Excited-state intramolecular proton-transfer (ESIPT) based fluorescence sensors and imaging agents. *Chem. Soc. Rev.* **2018**, *47*, 8842−8880.

(7) Magri, D. C.; Mallia, C. J. Metal ion sensing for biomedical uses. *Monogr. Supramol. Chem.* **2013**, *13*, 38−67.

(8) Vogel, E.; Köcher, M.; Schmickler, H.; Lex, J. Porphycene - a novel porphin isomer. *Angew. Chem., Int. Ed.* **1986**, *25*, 257−259.

(9) Braslavsky, S. E.; Müller, M.; Mártire, D. O.; Pörting, S.; Bertolotti, S. G.; Chakravorti, S.; Koç-Weier, G.; Knipp, B.; Schaffner, K. Photophysical properties of porphycene derivatives (18 π porphyrinoids). *J. Photochem. Photobiol., B* **1997**, *40*, 191−198.

(10) Waluk, J. Spectroscopy and tautomerization studies of porphycenes. *Chem. Rev.* **2017**, *117*, 2447−2480.

(11) Stockert, J.; Canete, M.; Juarranz, A.; Villanueva, A.; Horobin, R.; Borrell, J.; Teixido, J.; Nonell, S. Porphycenes: Facts and prospects in photodynamic therapy of cancer. *Curr. Med. Chem.* **2007**, *14*, 997−1026.

(12) Brenner, W.; Malig, J.; Costa, R. D.; Guldi, D. M.; Jux, N. Poly-ortho-functionalizable tetraarylporphycene platform-synthesis of octacationic derivatives towards the layer-by-layer design of versatile graphene oxide photoelectrodes. *Adv. Mater.* **2013**, *25*, 2314−2318.

(13) Oohora, K.; Ogawa, A.; Fukuda, T.; Onoda, A.; Hasegawa, J.-y.; Hayashi, T. *Meso*-Dibenzoporphycene has a large bathochromic shift and a porphycene framework with an unusual cis tautomeric form. *Angew. Chem., Int. Ed.* **2015**, *54*, 6227−6230.

(14) Kuzuhara, D.; Sakaguchi, M.; Furukawa, W.; Okabe, T.; Aratani, N.; Yamada, H. Synthesis, characterization and protonation behavior of quinoxaline-fused porphycenes. *Molecules* **2017**, *22*, 908.

(15) Planas, O.; Fernández-Llaneza, D.; Nieves, I.; Ruiz-Gonzalez, R.; Lemp, E.; Zanocco, A. L.; Nonell, S. Acid- and hydrogen-bonding-

induced switching between 22-pi and 18-pi electron conjugations in 2-aminothiazolo[4,5-c]porphycenes. *Phys. Chem. Chem. Phys.* **2017**, *19*, 25537−25543.
(16) Abe, M.; Futagawa, H.; Ono, T.; Yamada, T.; Kimizuka, N.; Hisaeda, Y. An electropolymerized crystalline film incorporating axially-bound metalloporphycenes: remarkable reversibility, reproducibility, and coloration efficiency of ruthenium(II/III)-based electrochromism. *Inorg. Chem.* **2015**, *54*, 11061−11063.
(17) Stępień, M.; Donnio, B.; Sessler, J. L. Discotic liquid-crystalline materials based on porphycenes: A mesogenic metalloporphycene-tetracyanoquinodimethane (TCNQ) adduct. *Chem.—Eur. J.* **2007**, *13*, 6853−6863.
(18) Ono, T.; Shinjo, H.; Koga, D.; Hisaeda, Y. Synthesis of a *meso*-tetraalkylporphycene bearing reactive sites: toward porphycene-polydimethylsiloxane hybrids with enhanced photophysical properties. *Eur. J. Org. Chem.* **2019**, *2019*, 7578−7583.
(19) Gil, M.; Dobkowski, J.; Wiosna-Sałyga, G.; Urbańska, N.; Fita, P.; Radzewicz, C.; Pietraszkiewicz, M.; Borowicz, P.; Marks, D.; Glasbeek, M.; Waluk, J. Unusual, solvent viscosity-controlled tautomerism and photophysics: *meso*-alkylated porphycenes. *J. Am. Chem. Soc.* **2010**, *132*, 13472−13485.
(20) Ciąćka, P.; Fita, P.; Listkowski, A.; Radzewicz, C.; Waluk, J. Evidence for dominant role of tunneling in condensed phases and at high temperatures: double hydrogen transfer in porphycenes. *J. Phys. Chem. Lett.* **2016**, *7*, 283−288.
(21) Ciąćka, P.; Fita, P.; Listkowski, A.; Kijak, M.; Nonell, S.; Kuzuhara, D.; Yamada, H.; Radzewicz, C.; Waluk, J. Tautomerism in porphycenes: analysis of rate-affecting factors. *J. Phys. Chem. B* **2015**, *119*, 2292−2301.
(22) Waluk, J. Tautomerization in porphycenes. In *Hydrogen-Transfer Reactions*; Hynes, J. T., Klinman, J. P., Limbach, H. H., Schowen, R. L., Eds.; Wiley-VCH: Weinheim, 2007; Vol. *1*, pp 245−271.
(23) Duran-Frigola, M.; Tejedor-Estrada, R.; Sánchez-García, D.; Nonell, S. Dual fluorescence in 9-amino-2,7,12,17-tetraphenylporphycene. *Phys. Chem. Chem. Phys.* **2011**, *13*, 10326−10332.
(24) Planas, O.; Tejedor-Estrada, R.; Nonell, S. Tautomerism and dual fluorescence in 9-substituted n-propyl- and methoxyethyl-porphycenes. *J. Porphyrins Phthalocyanines* **2012**, *16*, 633−640.
(25) Fita, P.; Garbacz, P.; Nejbauer, M.; Radzewicz, C.; Waluk, J. Ground and excited state double hydrogen transfer in symmetric and asymmetric potentials: comparison of 2,7,12,17-tetra-*n*-propylporphycene with 9-acetoxy-2,7,12,17-tetra-*n*-propylporphycene. *Chem.—Eur. J.* **2011**, *17*, 3672−3678.
(26) Fita, P.; Pszona, M.; Orzanowska, G.; Sánchez-García, D.; Nonell, S.; Vauthey, E.; Waluk, J. Tautomerization in 2,7,12,17-tetraphenylporphycene and 9-amino-2,7,12,17-tetraphenylporphycene: influence of asymmetry on the transition moment directaions. *Chem.—Eur. J.* **2012**, *18*, 13160−13167.
(27) Fita, P.; Urbańska, N.; Radzewicz, C.; Waluk, J. Ground and excited state tautomerization rates in porphycenes. *Chem.—Eur. J.* **2009**, *15*, 4851−4856.
(28) Waluk, J. Ground- and excited-state tautomerism in porphycenes. *Acc. Chem. Res.* **2006**, *39*, 945−952.
(29) Mengesha, E. T.; Zehnacker-Rentien, A.; Sepioł, J.; Kijak, M.; Waluk, J. Spectroscopic study of jet-cooled deuterated porphycenes: unusual isotopic effects on proton tunneling. *J. Phys. Chem. B* **2015**, *119*, 2193−2203.
(30) Mengesha, E. T.; Sepioł, J.; Borowicz, P.; Waluk, J. Vibrations of porphycene in the S_0 and S_1 electronic states: Single vibronic level dispersed fluorescence study in a supersonic jet. *J. Chem. Phys.* **2013**, *138*, 174201.
(31) Vdovin, A.; Sepioł, J.; Urbańska, N.; Pietraszkiewicz, M.; Mordziński, A.; Waluk, J. Evidence for two forms, double hydrogen tunneling, and proximity of excited states in bridge-substituted porphycenes: Supersonic jet studies. *J. Am. Chem. Soc.* **2006**, *128*, 2577−2586.
(32) Sepioł, J.; Stepanenko, Y.; Vdovin, A.; Mordziński, A.; Vogel, E.; Waluk, J. Proton tunnelling in porphycene seeded in a supersonic jet. *Chem. Phys. Lett.* **1998**, *296*, 549−556.
(33) Vdovin, A.; Waluk, J.; Dick, B.; Slenczka, A. Mode-selective promotion and isotope effects of concerted double-hydrogen tunneling in porphycene embedded in superfluid helium nanodroplets. *ChemPhysChem* **2009**, *10*, 761−765.
(34) Piwoński, H.; Stupperich, C.; Hartschuh, A.; Sepioł, J.; Meixner, A.; Waluk, J. Imaging of tautomerism in a single molecule. *J. Am. Chem. Soc.* **2005**, *127*, 5302−5303.
(35) Piwoński, H.; Sokołowski, A.; Kijak, M.; Nonell, S.; Waluk, J. Arresting tautomerization in a single molecule by the surrounding polymer: 2,7,12,17-tetraphenylporphycene. *J. Phys. Chem. Lett.* **2013**, *4*, 3967−3971.
(36) Piwoński, H.; Hartschuh, A.; Urbańska, N.; Pietraszkiewicz, M.; Sepioł, J.; Meixner, A.; Waluk, J. Polarized spectroscopy studies of single molecules of porphycenes: tautomerism and orientation. *J. Phys. Chem. C* **2009**, *113*, 11514−11519.
(37) Piatkowski, L.; Schanbacher, C.; Wackenhut, F.; Jamrozik, A.; Meixner, A. J.; Waluk, J. Nature of large temporal fluctuations of hydrogen transfer rates in single molecules. *J. Phys. Chem. Lett.* **2018**, *9*, 1211−1215.
(38) Gawinkowski, S.; Pszona, M.; Gorski, A.; Niedziółka-Jönsson, J.; Kamińska, I.; Nogala, W.; Waluk, J. Single molecule Raman spectra of porphycene isotopologues. *Nanoscale* **2016**, *8*, 3337−3349.
(39) Kumagai, T.; Hanke, F.; Gawinkowski, S.; Sharp, J.; Kotsis, K.; Waluk, J.; Persson, M.; Grill, L. Controlling intramolecular hydrogen transfer in a porphycene molecule with single atoms or molecules located nearby. *Nat. Chem.* **2014**, *6*, 41−46.
(40) Kumagai, T.; Hanke, F.; Gawinkowski, S.; Sharp, J.; Kotsis, K.; Waluk, J.; Persson, M.; Grill, L. Thermally and vibrationally induced tautomerization of single porphycene molecules on a Cu(110) surface. *Phys. Rev. Lett.* **2013**, *111*, 246101.
(41) Böckmann, H.; Liu, S.; Mielke, J.; Gawinkowski, S.; Waluk, J.; Grill, L.; Wolf, M.; Kumagai, T. Direct observation of photoinduced tautomerization in single molecules at a metal surface. *Nano Lett.* **2016**, *16*, 1034−1041.
(42) Fita, P.; Grill, L.; Listkowski, A.; Piwoński, H.; Gawinkowski, S.; Pszona, M.; Sepioł, J.; Mengesha, E.; Kumagai, T.; Waluk, J. Spectroscopic and microscopic studies of tautomerization in porphycenes: condensed phase, supersonic jets, and single molecule studies. *Phys. Chem. Chem. Phys.* **2017**, *19*, 4921−4937.
(43) Ladenthin, J. N.; Grill, L.; Gawinkowski, S.; Liu, S.; Waluk, J.; Kumagai, T. Hot carrier-induced tautomerization within a single porphycene molecule on Cu(111). *ACS Nano* **2015**, *9*, 7287−7295.
(44) Ladenthin, J. N.; Frederiksen, T.; Persson, M.; Sharp, J. C.; Gawinkowski, S.; Waluk, J.; Kumagai, T. Force-induced tautomerization in a single molecule. *Nat. Chem.* **2016**, *8*, 935−940.
(45) Koch, M.; Pagan, M.; Persson, M.; Gawinkowski, S.; Waluk, J.; Kumagai, T. Direct observation of double hydrogen transfer via quantum tunneling in a single porphycene molecule on a Ag(110) surface. *J. Am. Chem. Soc.* **2017**, *139*, 12681−12687.
(46) Sobolewski, A. L.; Gil, M.; Dobkowski, J.; Waluk, J. On the origin of radiationless transitions in porphycenes. *J. Phys. Chem. A* **2009**, *113*, 7714−7716.
(47) Urbańska, N.; Pietraszkiewicz, M.; Waluk, J. Efficient synthesis of porphycene. *J. Porphyrins Phthalocyanines* **2007**, *11*, 596−600.
(48) Vogel, E.; Köcher, M.; Lex, J.; Ermer, O. Steric modulation of the porphycene system by alkyl substituents: 9.10,19,20-Tetraalkylporphycenes. *Isr. J. Chem.* **1989**, *29*, 257−266.
(49) Czerski, I.; Listkowski, A.; Nawrocki, J.; Urbańska, N.; Piwoński, H.; Sokołowski, A.; Pietraszkiewicz, O.; Pietraszkiewicz, M.; Waluk, J. The long and winding road to new porphycenes. *J. Porphyrins Phthalocyanines* **2012**, *16*, 589−602.
(50) Lausmann, M.; Zimmer, I.; Lex, J.; Lueken, H.; Wieghardt, K.; Vogel, E. μ-Oxodiiron(III) complexes of porphycenes. *Angew. Chem., Int. Ed. Engl.* **1994**, *33*, 736−739.
(51) Nawara, K.; Waluk, J. Improved method of fluorescence quantum yield determination. *Anal. Chem.* **2017**, *89*, 8650−8655.
(52) Nawara, K.; Rana, A.; Panda, P. K.; Waluk, J. Versatile approach for reliable determination of both high and low values of luminescence quantum yields. *Anal. Chem.* **2018**, *90*, 10139−10143.

https://dx.doi.org/10.1021/acs.jpca.0c02155
J. Phys. Chem. A 2020, 124, 4594−4604

(53) Nawara, K.; Waluk, J. Goodbye to quinine in sulfuric acid solutions as a fluorescence quantum yield standard. *Anal. Chem.* **2019**, *91*, 5389−5394.
(54) Brouwer, A. M. Standards for photoluminescence quantum yield measurements in solution. *Pure Appl. Chem.* **2011**, *83*, 2213−2228.
(55) Magde, D.; Wong, R.; Seybold, P. G. Fluorescence quantum yields and their relation to lifetimes of rhodamine 6G and fluorescein in nine solvents: improved absolute standards for quantum yields. *Photochem. Photobiol.* **2002**, *75*, 327−334.
(56) Yanai, T.; Tew, D. P.; Handy, N. C. A new hybrid exchange-correlation functional using the Coulomb-attenuating method (CAM-B3LYP). *Chem. Phys. Lett.* **2004**, *393*, 51−57.
(57) Frisch, M. J.; Trucks, G. W.; Schlegel, H. B.; Scuseria, G. E.; Robb, M. A.; Cheeseman, J. R.; Scalmani, G.; Barone, V.; Mennucci, B.; Petersson, G. A.; et al. *Gaussian 09*, Revision B.01; Gaussian, Inc.: Wallingford CT, 2010.
(58) Frisch, M.; Trucks, G.; Schlegel, H.; Scuseria, G.; Robb, M.; Cheeseman, J.; Scalmani, G.; Barone, V.; Petersson, G.; Nakatsuji, H.; et al. *Gaussian 16*, Revision B.01; Gaussian, Inc.: Wallingford CT, 2016.
(59) Waluk, J.; Müller, M.; Swiderek, P.; Köcher, M.; Vogel, E.; Hohlneicher, G.; Michl, J. Electronic states of porphycenes. *J. Am. Chem. Soc.* **1991**, *113*, 5511−5527.
(60) Dobkowski, J.; Galievsky, V.; Starukhin, A.; Vogel, E.; Waluk, J. Spectroscopy and photophysics of tetraalkyldibenzoporphycenes. *J. Phys. Chem. A* **1998**, *102*, 4966−4971.
(61) Dobkowski, J.; Lobko, Y.; Gawinkowski, S.; Waluk, J. Energy relaxation paths in matrix-isolated excited molecules: comparison of porphycene with dibenzoporphycenes. *Chem. Phys. Lett.* **2005**, *416*, 128−132.
(62) Planas, O.; Gallavardin, T.; Nonell, S. Unusual properties of asymmetric porphycenes. *Handbook of Porphyrin Science, World Scientific*; Kadish, K. M., Smith, K. M., Guilard, R., Eds.; World Scientific, 2016; Vol. *41*, pp 299−349.
(63) Sinicropi, A.; Nau, W. M.; Olivucci, M. Excited-state quenching via "unsuccessful" chemical reactions. *Photochem. Photobiol. Sci.* **2002**, *1*, 537−546.
(64) Benoit, M.; Marx, D. The shapes of protons in hydrogen bonds depend on the bond length. *ChemPhysChem* **2005**, *6*, 1738−1741.
(65) Litman, Y.; Richardson, J. O.; Kumagai, T.; Rossi, M. Elucidating the nuclear quantum dynamics of intramolecular double hydrogen transfer in porphycene. *J. Am. Chem. Soc.* **2019**, *141*, 2526−2534.
(66) Gil, M.; Organero, J. A.; Waluk, J.; Douhal, A. Ultrafast dynamics of alkyl-substituted porphycenes in solution. *Chem. Phys. Lett.* **2006**, *422*, 142−146.

https://dx.doi.org/10.1021/acs.jpca.0c02155
J. Phys. Chem. A 2020, 124, 4594−4604